Fifth International Symposium on Marine Propulsors
smp'17, Espoo, Finland, June 2017

A Semi-Empirical Method to Predict Broadband Hull Pressure Fluctuations and Underwater Radiated Noise by Cavitating Tip Vortices

Johan Bosschers

Maritime Research Institute Netherlands (MARIN), Wageningen, The Netherlands

ABSTRACT

A semi-empirical method is presented that predicts broadband hull pressure fluctuations and underwater radiated noise due to propeller tip vortex cavitation. The method uses a hump-shaped pattern for the spectrum and it predicts the center frequency and level of this hump. The principal parameter is the vortex cavity size which is predicted using a combination of a boundary element method and a semi-empirical vortex model. It is shown that such a model is able to well represent the variation of cavity size with cavitation number. Using a database of model-scale and full-scale measured hull pressure data, an empirical formulation for the center frequency and level has been developed that is a function of among others the cavity size. Predicted and measured hull pressure and radiated noise spectra are compared for various cases. Acceptable results are obtained but the comparison also shows differences that require adjustments of parameters which need to be further investigated.

Keywords

Propeller, cavitation, tip vortex, hull pressures, underwater radiated noise

1 INTRODUCTION

Noise and vibration onboard ships are important for comfort of crew and passengers. Especially passengers on cruise vessels and owners of yachts require high comfort levels. An important source of noise and vibration is cavitation on the ship propeller. The collapse of cavitation generates pressure fluctuations that excite the ship hull above the propeller. Noise reduction is usually achieved by unloading the propeller tip and decreasing sheet cavitation as much as possible. This leaves often only tip vortex cavitation on the propeller. However, this type of cavitation generates broadband hull pressure fluctuations which may lead to ship vibration issues (Brubakk & Smogeli 1988, Carlton 2015).

The cavitating propeller is also an important contributor to the underwater radiated noise (URN) of ships. URN is relevant for the acoustic signature of military ships, the operation of equipment that require low self-noise such as sonar and for the influence on marine life. The latter used to be relevant for fishery research vessels only, but in the last decade the impact on the marine environment of URN due to shipping in general has received considerable attention. This has for instance resulted in EU sponsored projects on this area such as the SONIC project (Prins *et al*. 2016).

The spectrum of the broadband hull pressure fluctuations is characterized by a hump of which the maximum level increases with ship speed, while simultaneously the center of the hump moves to lower frequencies. The center frequency is typically located between 30 and 200 Hz. A possible explanation of the hump in the spectrum is that it is caused by a resonance frequency of the cavitating vortex (Bosschers 2009) but experimental evidence is missing. The proposed criterion for resonance assumes zero group speed in the dispersion relation for cavitating vortices. Experimental evidence for this dispersion relation is presented in Pennings *et al.* (2015a) in which also further support for the criterion for resonance is given. The relation between the broadband hull pressures and the higher order harmonics of the blade rate frequency is briefly discussed by Bosschers (2015a).

It has been shown that the source level of URN due to propeller cavitation has a direct relation with the pressure levels on the hull (Newman & Abrahamsen 2007, Foeth & Bosschers 2016). By correcting the hull pressures for the solid boundary factor on the hull and the distance between cavity collapse and pressure sensor, the source levels can directly be obtained from the measured hull pressures. These source levels are in reasonable agreement with the source levels as obtained by hydrophone measurements in the far field of the ship.

The hull pressure fluctuations and URN can be predicted in model basins such as the Depressurized Wave Basin (DWB) of MARIN (van Wijngaarden 2011, Bosschers *et al.* 2013, Lafeber & Bosschers 2016). CFD methods are rapidly developing but are still computationally expensive and not yet mature enough in this area to be used in the iterative design procedure. Rapid evaluation of propeller designs usually relies on the use of potential flow methods which can predict sheet cavitation and hull pressure fluctuations at the blade rate frequency (Bosschers *et al.* 2008). Because in potential flow methods vortices are fitted rather than captured, alternative methods are required to predict the nuisance

due to vortex cavitation. The present paper proposes a semi-empirical method for this purpose.

The method predicts the noise level and frequency of the center of the hump in the spectrum which are related to the tip vortex cavity size by an empirical relation that is presented in Section 2. The used formulations for the spectral shape for the source levels and the URN are presented in Section 3. Comparison of predicted and measured data is presented in Section 4.

2 PREDICTION OF THE CAVITY SOURCE STRENGTH

2.1 Introduction

The present method is based on the semi-empirical method to predict inboard noise of cavitating tip vortices by Raestad (1996). This method relates the noise to the size of the vortex cavity that is estimated from a potential flow method. In the present method use is made of the boundary element method PROCAL (Vaz & Bosschers 2006, Bosschers *et al.* 2008, Bosschers *et al.* 2015b) to estimate the vortex strength (circulation) of the tip vortex. This strength is used in a vortex model for the distribution of the azimuthal velocity to predict the cavity size for given cavitation number. This aspect is discussed in Section 2.2 and 2.3. The cavity size has been used to develop an empirical relation for the center frequency and level of the broadband hump. This procedure is presented in Section 2.4.

2.2 Vortex Models

To find the relation between cavitation number and cavity size for a vortex use is made of the azimuthal velocity v_θ only. It has been shown (Hommes *et al.* 2015) that the variation of pressure p with radius r can be computed within 10 to 15% accuracy using the relation

$$p - p_\infty = -\int_r^\infty \rho \frac{v_\theta^2}{r} dr \qquad (1)$$

Theoretical analysis has shown that the variation of cavity size with cavitation number for an analytical solution of a columnar cavitating vortex is almost identical to that of a non-cavitating vortex (Bosschers 2010). For the non-cavitating vortex, the cavity radius was taken as the radius where pressure equals vapour pressure. Therefore, only non-cavitating vortex models will be considered in the following.

The most simple vortex model is the potential flow vortex, which is a Rankine vortex without viscous core. The azimuthal velocity is given by

$$v_\theta(r,\theta) = \frac{\Gamma_\infty}{2\pi r} \qquad (2)$$

where Γ_∞ is the circulation at large r which equals the vortex strength. Disadvantage of this model, referred to in the following as Rankine vortex, is the singular behavior at the center which leads to an infinitely low pressure at that location. For practical applications this results in

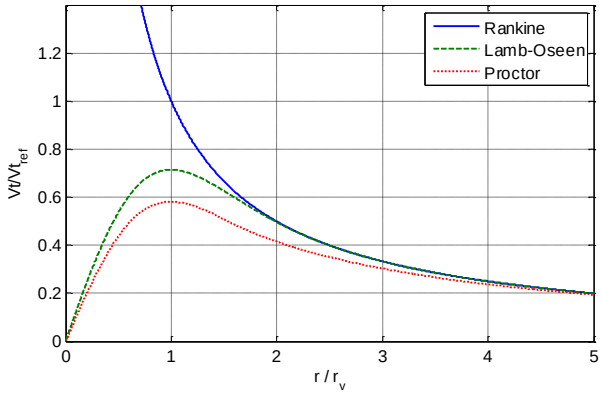

Figure 1. Non-dimensional azimuthal velocity distribution for various vortex models.

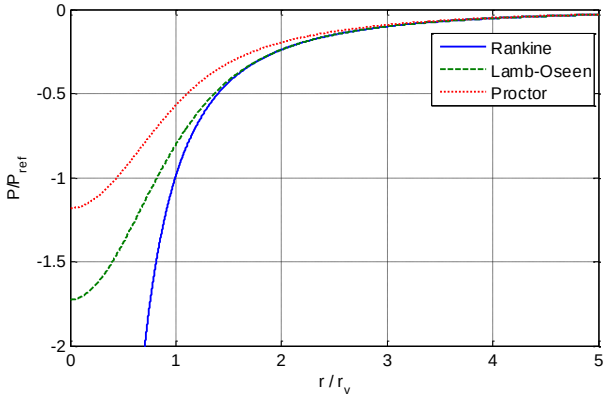

Figure 2. Non-dimensional pressure distribution for various vortex models.

cavitation inception just above zero ship speed. In real flow this singular behavior does not appear due to viscous effects. An analytical solution for a columnar vortex in laminar flow is the Lamb-Oseen vortex (Lamb 1993) with viscous core radius r_v:

$$v_\theta(r,\theta) = \frac{\Gamma_\infty}{2\pi r}\left\{1 - \exp\left[-\varsigma\left(r/r_v\right)^2\right]\right\} \qquad (3)$$

The parameter ς is a constant that is selected such that v_θ has its maximum value at $r = r_v$ which gives $\varsigma = 1.2564$. The Lamb-Oseen vortex can be interpreted as the solution of a potential flow vortex of which the vorticity has been distributed by diffusion. For trailing tip vortices, the distribution of vorticity is also influenced by the roll-up of the trailing vortex sheet that is generated by the circulation distribution on wing or propeller. The velocity distribution resulting from such a process has been proposed by Proctor *et al.* (2010) and is given by:

$$v_\theta(r,\theta) = \begin{cases} 1.0939\dfrac{\Gamma_\infty}{2\pi r}\left\{1 - \exp\left[-\beta\left(1.4\, r_v/B\right)^p\right]\right\} & \\ \qquad \times\left\{1 - \exp\left[-\varsigma\left(r/r_v\right)^2\right]\right\} & r \le 1.4\, r_v \\ \dfrac{\Gamma_\infty}{2\pi r}\left\{1 - \exp\left[-\beta\left(r/B\right)^p\right]\right\} & r > 1.4\, r_v \end{cases} \qquad (4)$$

In this formulation B is the length scale that is related to the vorticity roll-up region, taken as the half-span of the aircraft wing by Proctor. The parameters β and p are non-dimensional empirical parameters for which $\beta = 10$

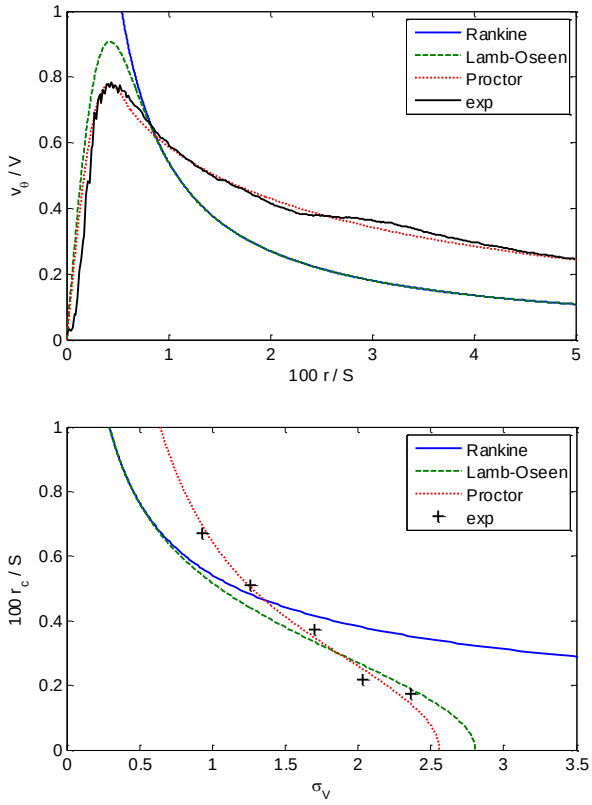

Figure 3. Measured and fitted azimuthal velocity distribution (top) and cavity size variation (bottom) for a wing of elliptical planform at 7 deg angle of attack. Experiments by Pennings *et al.* (2015b).

and $p = 0.75$ has been used. The variation of the azimuthal velocity with radius is presented in Figure 1 and the corresponding pressure distribution is presented in Figure 2. The parameter B was taken as $B/r_v = 20$.

2.3 Prediction of Cavity Size

The vortex models described in Section 2.2 have been evaluated using experimental datasets for a wing (Pennings *et al.* 2015b) and for a propeller (Kuiper 1981).

The dataset for the wing consists of velocity measurements obtained with particle image velocimetry at several stations downstream of the tip and of vortex cavity size measurements as function of cavitation number σ_V defined as

$$\sigma_V = \frac{p_w - p_v}{\frac{1}{2}\rho V^2} \tag{5}$$

with p_w the static pressure at the location of the wing, p_v the vapour pressure and V the free-stream velocity of the cavitation tunnel. The cavity size was obtained from image analysis. The wing was of elliptical planform (half-span $S/2 = 0.15\,\mathrm{m}$) and tested at three angles of attack. The velocities were averaged in circumferential direction and the resulting azimuthal velocity distribution for 7 deg angle of attack is presented in Figure 3 (top), which also shows the results of the vortex models. In these models,

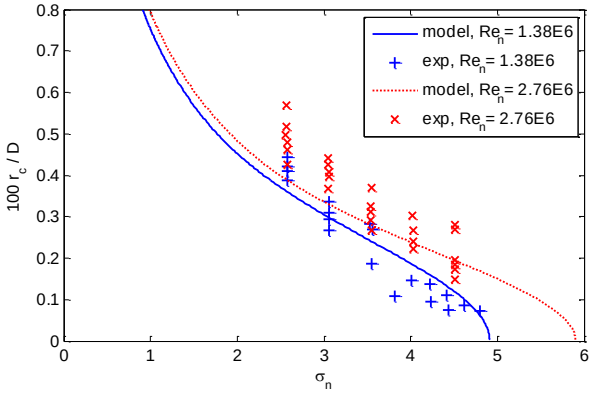

Figure 4. Measured and fitted variation of cavity size for a propeller at advance ratio J= 0.4. Experiments by Kuiper (1981).

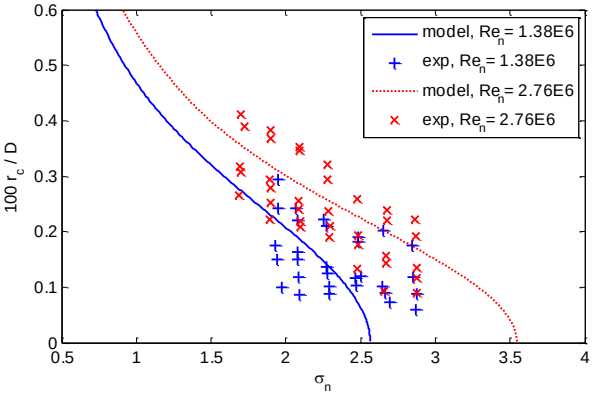

Figure 5. Measured and fitted variation of cavity size for a propeller at advance ratio J= 0.5. Experiments by Kuiper (1981).

r_v was taken from the radius with maximum value of v_θ in the experimental data. The Proctor vortex is able to fit the measured velocity distribution very well by tuning the coefficients for β and p. The vortex strength for the Proctor vortex was set to 80% of the maximum of the spanwise circulation distribution on the wing. This maximum value can be computed from the measured lift coefficient assuming that the circulation distribution is given by the analytical formulation. The resulting variation of cavity size with cavitation number of the Proctor vortex also shows very good agreement with experimental data (Figure 3, bottom). The Rankine and Lamb-Oseen vortex are not able to fit both the velocity distribution and the cavity size variation. In the results shown, the vortex strength for these vortices has been adapted such that the average cavity size is well predicted.

The data set for the propeller consists of the variation of cavity size with cavitation number σ_n defined as

$$\sigma_n = \frac{p_s - p_v}{\frac{1}{2}\rho n^2 D^2} \tag{6}$$

with p_s the static pressure at the shaft center, n the shaft rotation rate [rev/s] and D the propeller diameter. The propeller was specifically designed to show tip vortex cavitation only and has diameter $D = 0.34\,\mathrm{m}$. The

propeller was tested in open water conditions at three advance ratios by varying the free-stream velocity of the cavitation tunnel. Each advance ratio was tested at two shaft rotation rates resulting in two different Reynolds numbers. The cavity size was estimated using image analysis of photographs. On some of the propeller blades leading edge roughness was applied to stimulate cavitation inception.

The vortex strength was obtained from the circulation computed by PROCAL at 0.95R and the viscous core size was obtained from model-scale measurements by Jessup (1989) scaled according to equation (7), discussed later. Results will only be shown for the Proctor vortex model. Initially, the values for β and p were kept identical to the values obtained for the wing but these did not result in a good agreement with experimental data. This indicates that the vorticity roll-up of the wake of the propeller differs from that of the wing. A new tuning process was then applied for β and p which resulted in a reasonable agreement with experimental data, Figure 4 and Figure 5. The variation in Reynolds number in the experiments results in a different value for r_v in the vortex model. In the present method this dependency was taken into account by using the Reynolds number scaling for cavitation inception of McCormick (1962). The viscous core size can then be computed from the reference value of Jessup by:

$$\frac{r_v}{c} = \left(\frac{r_v}{c}\right)_{ref} \left(\frac{\mathrm{Re}}{\mathrm{Re}_{ref}}\right)^{-m/2} \tag{7}$$

with c the chord length and Re the Reynolds number for the chord length and the resultant velocity at 0.95R. The value for parameter m is computed using the formulation by Shen *et al.* (2009) resulting in a value of 0.38 and 0.37 for the lower and higher Reynolds number, respectively. The influence of the change in Reynolds number on cavity size is well predicted by this method.

Results were also analyzed for the other angles of attack for the wing and other advance ratios for the propeller. Good agreement was obtained for the two lowest angles of attack and the two highest advance ratios using the same settings for the vortex model. However, for the highest angle of attack and lowest advance ratio the predicted cavity size was smaller than observed in measurements. A possible reason for this underprediction is that in the experiment the vortex detachment location was shifted from the tip along the leading edge to a lower radial position which may lead to a combination of sheet and vortex cavitation. Unfortunately, no detailed images are available for these conditions.

2.4 Prediction of Source Strength

The tuning of the center frequency and level of the hump was performed using non-dimensional values. In the present study, use has been made of a combination of model-scale (measured in the DWB) and full-scale

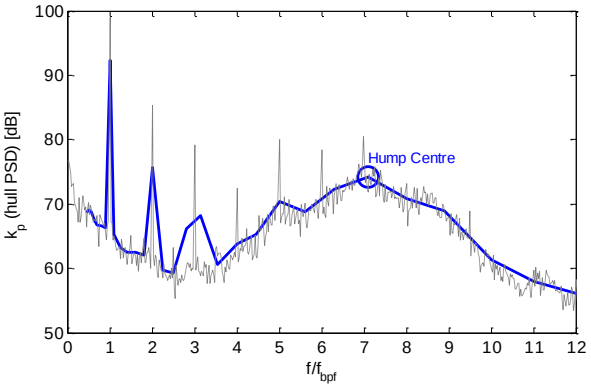

Figure 6. Example of a non-dimensional hull pressure power density spectrum of a two bladed research propeller. The solid line is the 1/6 octave band smoothened spectrum.

experimental data for hull pressures obtained on twin-screw vessels. The rms pressure amplitudes were converted into k_p-values according to equation (8) where Δf corresponds to the resolution bandwidth of the amplitude spectrum and f_{bpf} to the blade passage frequency. The levels were converted to decibel values according to equation (9). The frequencies were made non-dimensional with f_{bpf}.

$$k_p = \frac{p_{rms}}{\rho n^2 D^2 \sqrt{\Delta f \,/\, f_{bpf}}} \tag{8}$$

$$k_p\,[dB] = 120 + 20\log_{10}\left(k_p\right) \tag{9}$$

The resulting spectrum can then be interpreted as a non-dimensional power density spectrum or non-dimensional rms amplitude density spectrum. The hull pressure spectra were converted to source levels by correcting for the propeller-hull clearance and the solid boundary factor. Only the center pressure sensor located directly above the 12 o'clock position of the propeller was considered, as measurements at this location were available for all data sets.

To focus on the broadband character, the spectrum was converted to 1/6 octave band levels and scaled back to a power density spectrum (Figure 6). The resulting spectrum then becomes a smoothened power density spectrum. Next, the center frequency, the center (maximum) level and the bandwidth of the hump were determined by a curve fit and these values were used for the fitting process. In Figure 6, the fitted center frequency equals $f_c / f_{bpf} = 7.3$.

The parameters for the fitting process are the cavity size r_c made non-dimensional with diameter D, the cavitation number σ_n and the number of blades Z. The empirical relation for the centre (maximum) level is given by

$$k_{p,\max} = a_p + 20\log_{10}\left\{\left(\frac{r_c}{D}\right)^{\kappa}\sqrt{Z}\right\} \tag{10}$$

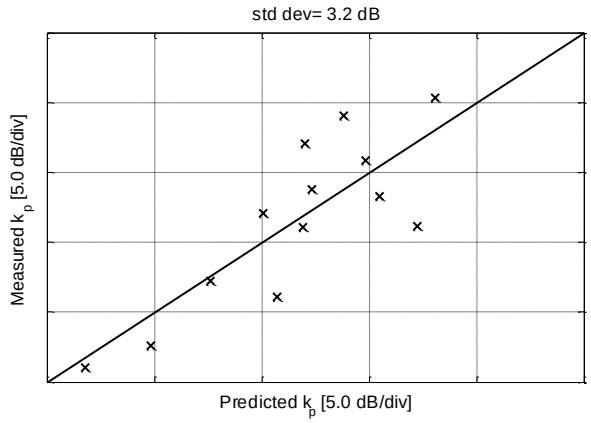

Figure 7. Comparison between measured and predicted center level of the hump for propellers dominated by tip vortex cavitation.

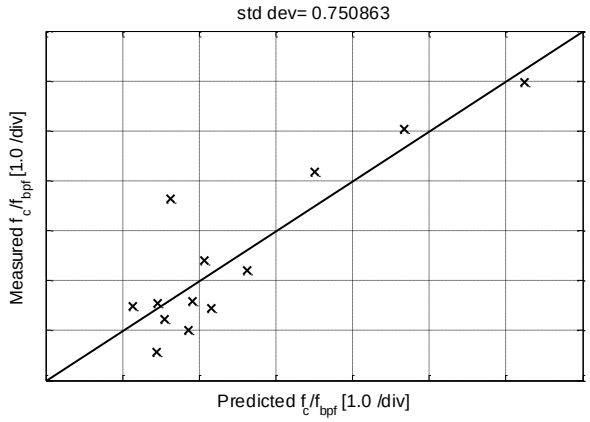

Figure 8. Comparison between measured and predicted center frequencies for propellers dominated by tip vortex cavitation.

in which the non-dimensional empirical constants a_p and κ were obtained by curve fitting. Raestad has used $\kappa = 2$ in his formulation but the value $\kappa = 3$ is used in the present method as this is closer to the trend seen in the datasets. The contribution from the total number of blades was summed as a set of incoherent sources. The formulation for the center frequency is based on theoretical considerations and is given by

$$\frac{f_c}{f_{bpf}} = b_f \frac{1}{r_c/D} \frac{\sqrt{\sigma_n}}{Z} \tag{11}$$

with b_f a non-dimensional empirical constant. Raestad derives this relation from the resonance frequency of a bubble but the relation has also been derived from the dispersion relation for a cavitating vortex (Bosschers 2009).

The vortex strength for the vortex models was obtained from the circulation value at 0.95R obtained by PROCAL. Use has been made of model-scale measured wake fields. For analysis of sea trial conditions, these were scaled using methods developed in Cooperative Research Ships (CRS) working groups (Hally, 2002).

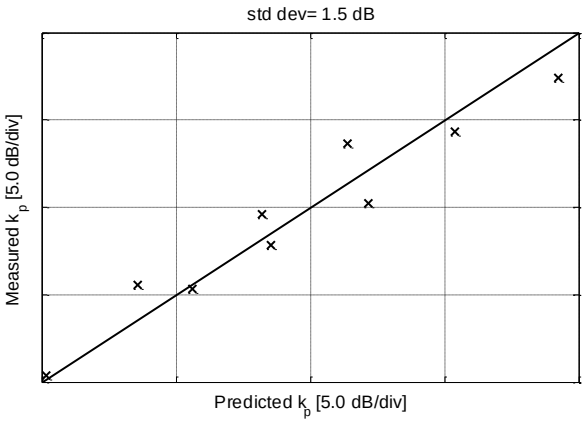

Figure 9. Comparison between measured and predicted center level of the hump for a two-bladed research propeller tested at various advance ratios and cavitation numbers.

During the process of fitting the data it became apparent that the experimental datasets had to be divided in separate groups. In the end a distinction was made between cases for which tip vortex cavitation was dominant and cases for which also sheet cavitation was present. This behavior was also observed in the fit of the cavity size as discussed in Section 2.3. Results for the cases dominated by vortex cavitation are presented in Figure 7 for the maximum level of the hump and in Figure 8 for the center frequency. An example of the noise level fit for an individual data set, not included in Figure 7, is presented in Figure 9. The propeller is a two-bladed research propeller tested for a range of cavitation numbers and thrust coefficients (Bosschers 2009). All results presented in Figure 7 through 9 are for the Proctor vortex model but similar results were obtained for the other vortex models. The results are quite reasonable although the standard deviation of the frequency is rather high; Especially one condition is poorly predicted.

The relation of the hump center level and frequency to cavity size can easily be converted to a relation in terms of propeller thrust coefficient for the (inviscid) Rankine vortex model. The relation between cavity size, cavitation number and circulation for this vortex is given by:

$$\frac{r_c}{D} = \frac{1}{2\pi} \frac{\Gamma_\infty}{nD} \frac{1}{\sqrt{\sigma_n}} \tag{12}$$

The non-dimensional vortex strength can be written as the product of the propeller blade thrust coefficient K_T/Z and a tip loading parameter τ. The following relations are then obtained for the center (maximum) level and center frequency

$$k_{p,\max} \propto \left(\frac{r_c}{D}\right)^{\kappa} \sqrt{Z} \propto \left(\frac{\tau K_T}{Z\sqrt{\sigma_n}}\right)^{\kappa} \sqrt{Z} \tag{13}$$

$$\frac{f_c}{f_{bpf}} \propto \frac{1}{r_c/D} \frac{\sqrt{\sigma_n}}{Z} \propto \frac{\sigma_n}{\tau K_T} \tag{14}$$

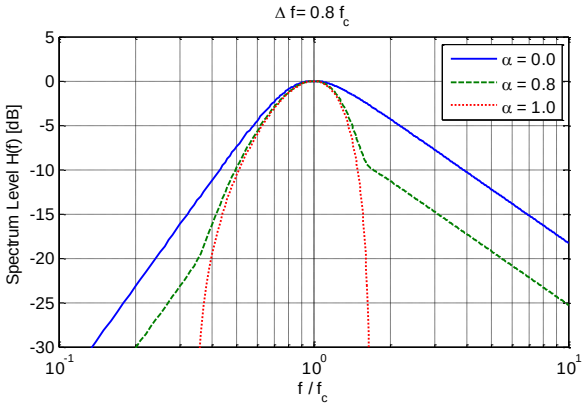

Figure 10. Examples of the shape of the spectrum for different values of α.

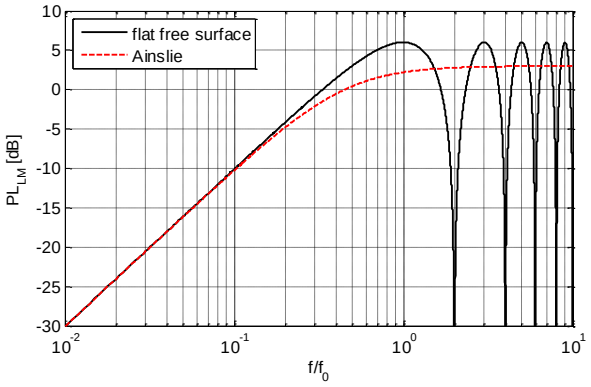

Figure 11. Propagation loss due to the Lloyd-mirror effect.

3 SHAPE OF THE SPECTRUM

3.1 Source Level

The shape of the spectrum of cavitation noise is described by e.g. Fitzpatrick & Strasberg (1958) and Blake (1986). The spectrum can be divided in a low frequency part and a high frequency part. The low frequency part is characterized by a hump due to the overall growth, collapse and rebounds of the cavity. The high frequency part is related to the final phase of the collapse process during which velocities may approach or exceed the speed of sound and compressibility effects become important. The collapse and rebounds of the smaller size bubbles generated by the collapse of the large scale structure may also contribute to the high frequency part.

In the present model it is assumed that f_c is related to a resonance frequency of the cavitating vortex. The related pressure signal can then be interpreted as a damped oscillatory signal, or as an oscillatory signal multiplied with a rectangular window. The Fourier transform of the latter is given by a sinc-function. Therefore, the shape of the spectrum, presented in decibel values, has been defined as

$$H_h(f) = 20\log_{10}\left\{\mathrm{sinc}\left(\frac{f - f_c}{0.830\,\Delta f_{-6dB}}\right)\right\} \qquad (15)$$

where Δf_{-6dB} corresponds to the half-power bandwidth. A small value for Δf_{-6dB} corresponds to a time trace with multiple rebounds (small damping) resulting in a narrow hump in the spectrum. A large value for Δf_{-6dB} corresponds to a highly damped system resulting in a wide hump in the spectrum. Analysis of experimental data showed that Δf_{-6dB} is proportional to f_c although the scatter is high.

The shape of the spectrum at very low and high frequencies relative to the center frequency of the hump is modeled separately. The simple model used here consists of prescribed slopes at low and high frequency in a power density spectrum:

$$H_s(f) = 10\log_{10}\left\{\frac{2(f/f_c)^{\alpha_l}}{1+(f/f_c)^{\alpha_l-\alpha_h}}\right\} \qquad (16)$$

in which α_h corresponds to the slope for high frequency, with typical value $\alpha_h = -2$, and α_l corresponds to the slope for low frequency, for which a value $\alpha_l = 4$ is used as suggested by Fitzpatrick & Strasberg. It is remarked that the maximum value of H_s is different from 0 dB which needs to be corrected for.

The resulting spectrum is then taken as a weighted sum of powers of the two spectral functions:

$$H(f) = 10\log_{10}\left\{\alpha 10^{H_h(f)/10} + (1-\alpha)10^{H_s(f)/10}\right\} \qquad (17)$$

where α is a user defined parameter. For practical applications this parameter is defined as

$$\Delta L_\alpha = 10\log_{10}(1-\alpha) \qquad (18)$$

with ΔL_α the difference in noise level between the maximum of the two-slope function and the maximum of the hump.

Examples of the shape of the spectrum for the source level are given in Figure 10 for three values of α, where the curve for $\alpha = 0.0$ shows the spectrum for the two-slope function and the curve for $\alpha = 1.0$ shows the spectrum by the sinc function. The maximum absolute value of the argument of the sinc function has been limited to avoid the presence of 'sidelobes' in the spectrum. In its current version the half-power bandwidth is a constant fraction of the center frequency and $\alpha = 0.8$. For some cases however, these defaults do not give a good representation of the measured spectrum and further research is required.

3.2 Hull Pressure and Radiated Noise Level

The hull pressure spectrum is obtained from the source level spectrum by correcting for a solid boundary factor and for the propeller-hull clearance. The spectrum of the underwater radiated noise levels is obtained from the source level spectrum by correcting for the interference with the free surface (Lloyd-mirror). A simple formula to

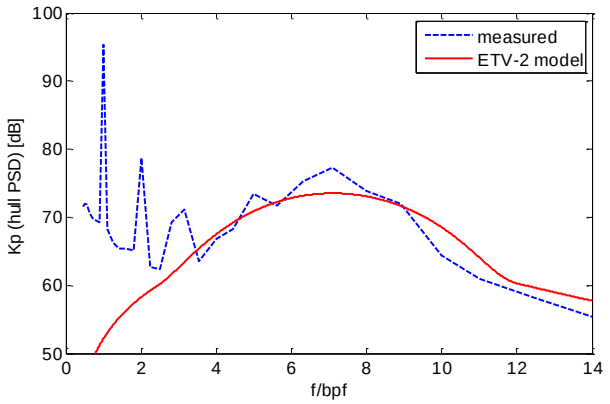

Figure 12. Example of the measured and predicted non-dimensional hull pressure spectrum for a two-bladed research propeller.

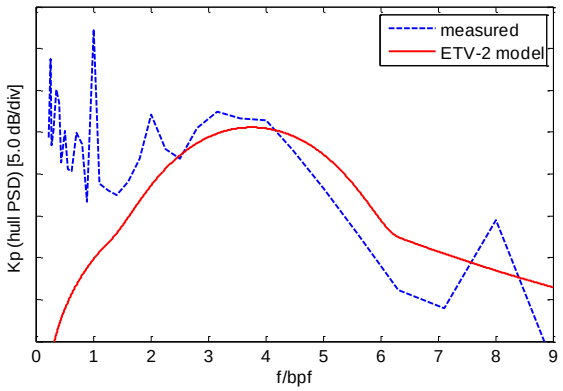

Figure 13. Example of the measured and predicted non-dimensional hull pressure spectrum for a ship propeller of the database tested at model scale.

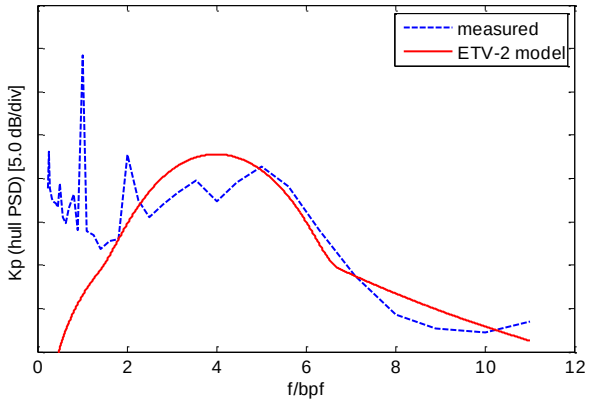

Figure 14. Example of the measured and predicted non-dimensional hull pressure spectrum for a ship propeller of the database tested at full scale.

correct for the propagation loss PL due to Lloyd-mirror is given by Ainslie (2010):

$$PL_{LM} = -10\log_{10}\left[\frac{1}{2}+\frac{1}{4k^2 d_s^2 \sin^2\theta}\right] \qquad (19)$$

where k corresponds to the acoustic wave number, d_s to the submergence depth of the cavity collapse and θ to the hydrophone depression angle. The function is compared to the theoretical formulation of the Lloyd-mirror effect for a flat free surface (Medwin & Clay 1998) in Figure 11. The frequency is made non-dimensional with the critical frequency f_0 given by

$$f_0 = \frac{c}{4d_s \sin\theta} \qquad (20)$$

where c corresponds to the speed of sound. The interference patterns at frequencies above the critical frequency are usually not observed in ship noise data because of the presence of waves and bubbles near the free surface. For that reason the Ainslie model assumes that at high frequencies the free surface leads to an uncorrelated image source.

The source level spectrum SL can now be defined as

$$SL(f) = L_{p,\max} + H(f) \quad \left[\text{dB, re}1\mu\text{Pa}^2\text{m}^2/\text{Hz}\right] \qquad (21)$$

with $L_{p,\max}$ the level of the center of the hump of the power density spectrum which is the dimensional value of $k_{p,\max}$. The spectrum of the underwater radiated noise level RNL is computed from the SL by correcting for Lloyd-mirror:

$$RNL(f) = SL(f) + PL_{LM}(f)\left[\text{dB, re}1\mu\text{Pa}^2\text{m}^2/\text{Hz}\right] \qquad (22)$$

The RNL levels, or URN levels in general, are often presented in one-third-octave band levels denoted by $RNL_{1/3}$ and $URN_{1/3}$, respectively.

The present method is referred to as ETV-2, the 2nd version of the Empirical Tip Vortex cavitation method.

4 PREDICTING HULL PRESSURES AND RADIATED NOISE

4.1 Hull pressures

An example of the resulting spectrum of hull pressures predicted by the ETV model for the two-bladed research propeller is presented in Figure 12. Overall, the hump is well represented by the default spectral shape. The fit for the center level and frequency was obtained from a dedicated fit to the test series for this propeller. The fit for the level is given in Figure 9.

Examples of spectra for ship configurations used in the database are presented for model scale and full scale in Figure 13 and Figure 14, respectively. Both cases are part of the fitting procedure presented in Figure 7 and Figure 8. The model-scale test results show some disturbance at the eighth harmonic of the blade passage frequency generated by the propeller driving train. However, this is located at a much higher frequency than the broadband hump due to the cavitating tip vortex. Both figures are examples of cases that are well predicted by the model. As shown in Figure 7 and Figure 8 there are also some cases for which the center level and frequency are predicted less accurately.

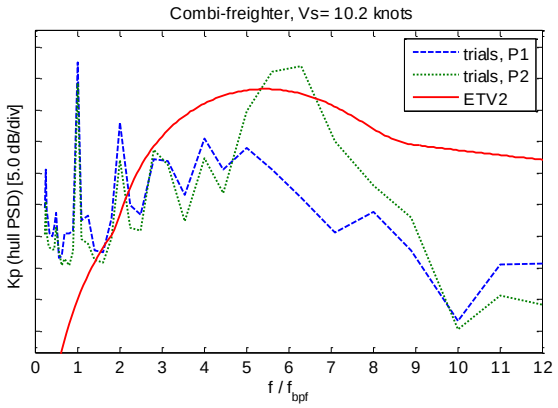

Figure 15. Measured and predicted non-dimensional hull pressure spectrum for the combi-freighter. P1 corresponds to the center transducer and P2 is located closer to the cavity collapse.

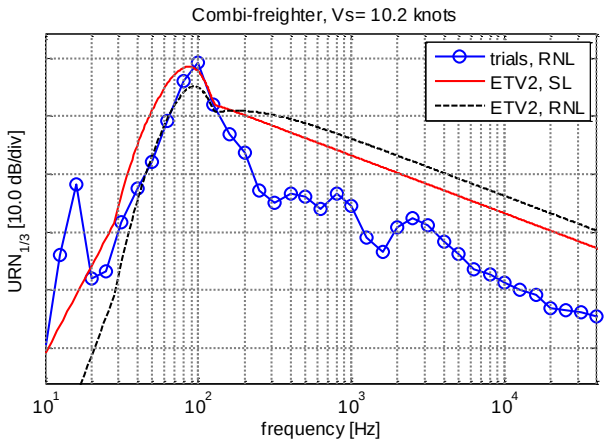

Figure 16. Measured and predicted radiated noise spectrum in one-third octave band levels for the combi-freighter using default values for the prediction model.

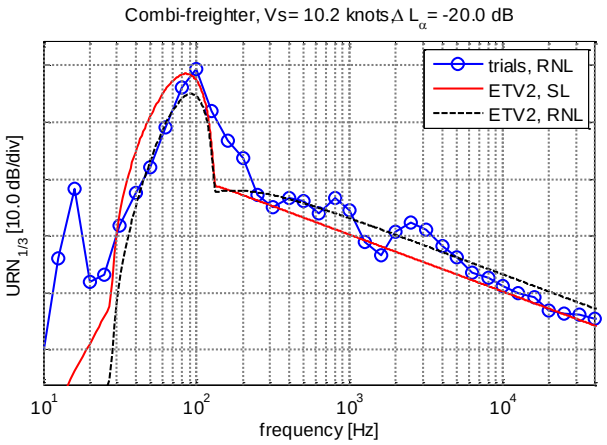

Figure 17. Measured and predicted radiated noise spectrum in one-third octave band levels for the combi-freighter using adapted value for ΔL_α .

The model-scale and full-scale data are all made non-dimensional using equation (8). Because no significant differences in the trend of the center level and frequency with ship scale could be discerned, it is concluded that equation (8) can be used to scale the broadband pressure spectra from model scale to full scale. Actually, the equation can also be obtained by rewriting the formulation that is used to scale the (low frequency) URN by cavitation as presented by e.g. Strasberg (1977) and Bark (1985).

The ETV-model has also been applied to predict the broadband hull pressure levels on a 85 m combi freighter equipped with a single controllable pitch propeller. This ship was not in the database and, being a single screw vessel, it also does not resemble any ship in the data base. The sea trials for the ship, which included URN measurements, were performed by DAMEN, DNV and MARIN and were financed by the CRS BROADBAND2 working group. The effective wake field for the PROCAL computation was obtained from a coupled RANS-BEM procedure (Rijpkema *et al.* 2013). The cavitation pattern on the propeller was characterized by strong tip vortex cavitation. The empirical constants for the complete database were applied in the ETV method.

The comparison of broadband hull pressures predicted by the ETV method and measured during the sea trial at 10 knots is reasonable (Figure 15). Remarkable is that the hump for this single screw ship is overpredicted by the ETV method. The URN of this vessel is dominated by a very pronounced hump that will be discussed later. This hump is not so obvious in the pressures measured by the center transducer (P1) but can clearly be seen in the spectrum of the pressure sensor located closer to the collapse of the vortex (transducer P2).

In general, the results were considered to be quite acceptable for a range of pitch settings and shaft rotation rates as long as the cavitation was present on the back side of the blade. In its present form the model was not able to predict the broadband pressure spectrum due to face side cavitation.

4.2 Underwater Radiated Noise

The model that was developed using data for hull pressures has also been applied to predict the URN due to propeller cavitation.

The first test case considered for the prediction of URN is the combi freighter discussed above. The noise levels are presented in Figure 16 using the default values. The center of the hump is well predicted in terms of level and frequency, but at high frequencies the predicted noise levels are approximately 10 dB too high. It is seen that the hump is very pronounced. The change in noise levels between the hump and the high frequency region can easily be adjusted with the parameter ΔL_α. Results for $\Delta L_\alpha = -20$ dB are presented in Figure 17. The default value for the slope of the spectrum at high frequencies is in good agreement with the sea trial data.

The second data set that will be analyzed is that of the (twin screw) cruise vessel MS Statendam as reported by Kipple (2002). The length between perpendiculars is 182 m and the ship is driven by controllable pitch propellers. The measured SL are directly taken from Kipple and the RNL are computed from the received noise levels at 500

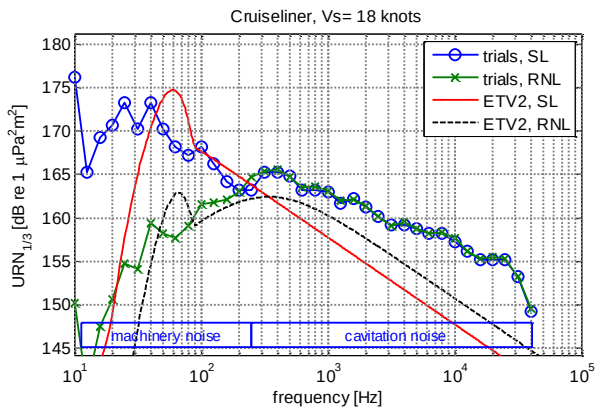

Figure 18. Measured and predicted radiated noise spectrum in one-third octave band levels for the cruise vessel using default values for the prediction model.

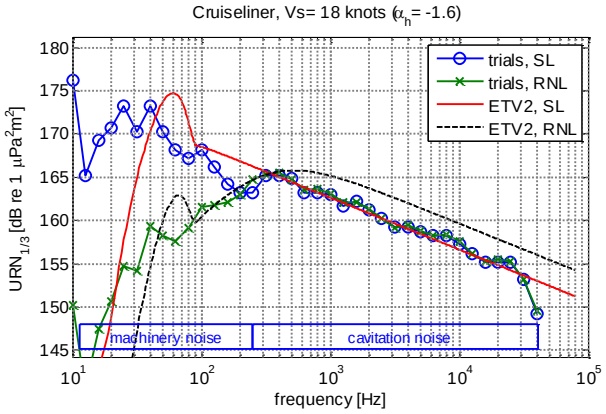

Figure 19. Measured and predicted radiated noise spectrum in one-third octave band levels for the cruise vessel using adapted values for the high frequency slope parameter α_h.

yard as reported by Kipple. All measured levels are converted to levels at 1 m distance assuming spherical spreading loss. The applied formulation to compute the source levels from the measured radiated noise levels is unknown but the difference in results is similar to those given by equation (19) except for high frequencies where the applied correction is 0 dB instead of 3 dB.

Results with default values are presented in Figure 18. The maximum level is very well predicted but the measured values in that frequency region are reported to be mainly due to machinery noise. At high frequencies, the agreement is not as good because the assumed slope of the spectrum is smaller than in the experiments. Adjustment of the high frequency slope to $\alpha_h = -1.6$ gives good agreement (Figure 19).

5. CONCLUDING REMARKS

A semi-empirical method to predict broadband hull pressure fluctuations and radiated noise by cavitating tip vortices has been presented. The method makes use of results obtained by a potential flow code and can therefore very easily be used for propeller noise evaluation, for instance in a propeller design process. The principal parameter in the method is the vortex cavity size from which the maximum noise level and its frequency is computed. Results show acceptable agreement with sea trial data that was not used to develop the empirical relations.

During the development and application of the method a number of issues were identified that require further investigation. An important aspect is the contribution of sheet cavitation and the interaction between sheet and tip vortex cavitation in the generation of the broadband hump. Another aspect is the overall shape of the spectrum, in particular the relation between the levels of the hump and the levels at the high frequency region. Also physical aspects that influence the slope of the high frequency noise require further investigation.

ACKNOWLEDGEMENTS

The present work has been performed within the Cooperative Research Ships (CRS) BROADBAND and BROADBAND2 working group, www.crships.org.

REFERENCES

Ainslie, M. (2010). 'Principles of Sonar Performance'. Springer-Praxis.

Bark G. (1985). 'Prediction of Propeller Cavitation Noise from Model Tests and its Comparison with Full Scale Data'. Journal of Fluids Engineering, Vol. 107.

Blake, W.K. (1986), 'Mechanics of Flow-Induced Sound and Vibration'. Academic Press.

Bosschers, J., G. Vaz, G., Starke, A.R. & van Wijngaarden, E. (2008), 'Computational Analysis of Propeller Sheet Cavitation and Propeller-Ship Interaction'. RINA conference MARINE CFD2008, Southampton, UK.

Bosschers J. (2009). 'Investigation of Hull Pressure Fluctuations Generated by Cavitating Vortices'. First international symposium on marine propulsors SMP'09, Trondheim, Norway.

Bosschers, J. (2010). 'On the Influence of Viscous Effects on 2-D Cavitating Vortices'. 9th International Conference on Hydrodynamics", Shanghai, China.

Bosschers, J., Lafeber, F.H., de Boer, J., Bosman, R. & Bouvy, A. (2013). 'Underwater Radiated Noise Measurements with a Silent Towing Carriage in the Depressurized Wave Basin'. Symposium on Advanced Measurement Techniques, AMT'13, Gdansk, Poland.

Bosschers, J. (2015a). 'On the Relation between Tonal and Broadband Content of Hull Pressure Spectra due to Cavitating Ship Propellers", 9th International Conference on Cavitation (CAV2015), Lausanne, Switzerland, Journal of Physics: Conference Series 656.

Bosschers, J., Willemsen, C., Peddle, A. & Rijpkema, D. (2015b). 'Analysis of Ducted Propellers by Combining Potential Flow and RANS Methods". Fourth International Symposium on Marine Propellers, SMP'15, Austin, Texas

Brubakk, E. & Smogeli, H. (1988). 'QE2 from Turbine to Diesel – Consequences for Noise and Vibration'. IMAS Conference, The design and development of passenger ships.

Carlton, J.S. (2015). 'Broadband Cavitation Excitation in Ships'. Ships and Offshore Structures 10:3.

Fitzpatrick, H.M. & Strasberg, M. (1956). 'Hydrodynamic Sources of Sound', First Symposium on Naval Hydrodynamics.

Foeth, E.J. & Bosschers, J. (2016). 'Localization and Source-Strength Estimation of Propeller Cavitation Noise using Hull Mounted Pressure Transducers'. 31st Symposium on Naval Hydrodynamics, Monterey, California, September 2016

Hally, D. (2002). 'User's guide for PIF_WAKE: The CRS PIF Wake Scaling Program for single and twin screw forms'. DRDC Atlantic Report ECR 2002-053.

Hommes, T., Bosschers, J. & Hoeijmakers, H.W.M. (2015). 'Evaluation of the Radial Pressure Distribution of Vortex Models and Comparison with Experimental Data'. 9th International Symposium on Cavitation CAV2015, Journal of Physics: Conference Series 656.

Jessup, S.D. (1989). 'An Experimental Investigation of Viscous Aspects of Propeller Blade Flow'. PhD thesis, The Catholic University of America, Washington D.C., USA.

Kipple, B. (2002). 'Southeast Alaska Cruise Ship Underwater Acoustic Noise'. Technical Report NSWCCD-71-TR-2002/574, Naval Surface Warfare Center Carderock Division, USA.

Kuiper, G. (1981). 'Cavitation Inception on Ship Propeller Models'. PhD thesis, Delft University of Technology, Delft, The Netherlands.

Lafeber F.H. & Bosschers, J. (2016), 'Validation of Computational and Experimental Prediction Methods for the Underwater Radiated Noise of a Small Research Vessel'. Proceedings of PRADS 2016, Copenhagen, Denmark.

Lamb, H. (1993). 'Hydrodynamics'. 6th Edition, Cambridge University Press

Mc Cormick (1962). 'On Cavitation Produced by a Vortex Trailing from a Lifting Surface'. Journal of Basic Engineering, September.

Medwin, H. & Clay, C.S. (1998). 'Fundamentals of Acoustical Oceanography'. Academic Press.

Newman, M. & Abrahamsen, K. (2007). 'Measurement of Underwater Noise'. Ship Noise and Vibration Conference, London, UK.

Pennings, P.C., Bosschers, J., Westerweel, J. & van Terwisga, T.J.C. (2015a). 'Dynamics of Isolated Vortex Cavitation'. Journal of Fluid Mechanics, Vol. 778, pp. 288-313.

Pennings, P.C., Westerweel, J. & van Terwisga, T.J.C. (2015b). 'Flow Field Measurements around Vortex Cavitation'. Exp. Fluids 56;206.

Prins, H.J. *et al.* (2016). 'Suppression of Underwater Noise Induced by Cavitation: SONIC'. Proceedings of the 6th Transport Research Arena, Warsaw, Poland.

Proctor, F.H., Ahmad, N.N., Switzer, G.S. & Limon Duparcmeur, F.M. (2010). 'Three-Phased Wake Vortex Decay'. AIAA Atmospheric and Space Environments Conference, AIAA 2010-7991, Toronto, Canada.

Raestad, A-E (1996). 'Tip Vortex Index – an Engineering Approach to Propeller Noise Prediction'. The Naval Architect, July/August.

Rijpkema, D., Starke, B. & Bosschers, J. (2013). 'Numerical Simulation of Propeller-Hull Interaction and Determination of the Effective Wake Field using a Hybrid RANS-BEM Approach'. Third International Symposium on Marine Propellers, smp'13, Launceston, Tasmania, Australia.

Shen, Y.T., Gowing, S. & Jessup, S. (2009). 'Tip Vortex Cavitation Inception Scaling for High Reynolds Number Applications'. Journal of Fluids Engineering, Vol. 131.

Strasberg M. (1977). 'Propeller Cavitation Noise after 35 Years of Study'. ASME Symposium on Noise and Fluid Engineering, pp 89-99, Netherlands.

Vaz, G. & Bosschers, J. (2006). 'Modeling Three Dimensional Sheet Cavitation on Marine Propellers using a Boundary Element Method'. Sixth International Symposium on Cavitation CAV2006, Wageningen, The Netherlands.

Van Wijngaarden, E. (2011). 'Prediction of Propeller-Induced Hull-Pressure Fluctuations'. PhD thesis, TU Delft, the Netherlands.

DISCUSSION

Question from Nobuhiro Hasuike

How do you take account of effects of differences in ship wake distribution ?

Author's closure

The ETV-model makes use of an estimate of the tip vortex strength by the boundary element method PROCAL by considering the circulation near the tip. As the ship wake field is used as input for PROCAL, the influence of the ship wake on tip vortex strength is taken into account through potential flow modeling. The influence of tip vortex strength on radiated noise is then taken into account by the ETV-model.